Northumbria Research Link

Citation: Zhao, Jinyan, Shi, Quanqi, Tian, Anmin, Shen, Xiao-Chen, Weygand, James M, Wang, Huizi, Yao, Shutao, Ma, Xiao, Degeling, Alexander William, Rae, Jonathan, Zhang, Hui, Zhang, Xiao-Jia, Bai, Shi-Chen, Shang, Wensai and Park, Jong-Sun (2021) Vortex Generation and Auroral Response to a Solar Wind Dynamic Pressure Increase: Event Analyses. Journal of Geophysical Research: Space Physics, 126 (3). e2020JA028753. ISSN 2169-9380

Published by: American Geophysical Union

URL: https://doi.org/10.1029/2020ja028753 <https://doi.org/10.1029/2020ja028753>

This version was downloaded from Northumbria Research Link: http://nrl.northumbria.ac.uk/id/eprint/45522/

Northumbria University has developed Northumbria Research Link (NRL) to enable users to access the University's research output. Copyright © and moral rights for items on NRL are retained by the individual author(s) and/or other copyright owners. Single copies of full items can be reproduced, displayed or performed, and given to third parties in any format or medium for personal research or study, educational, or not-for-profit purposes without prior permission or charge, provided the authors, title and full bibliographic details are given, as well as a hyperlink and/or URL to the original metadata page. The content must not be changed in any way. Full items must not be sold commercially in any format or medium without formal permission of the copyright holder. The full policy is available online: http://nrl.northumbria.ac.uk/policies.html

This document may differ from the final, published version of the research and has been made available online in accordance with publisher policies. To read and/or cite from the published version of the research, please visit the publisher's website (a subscription may be required.)

Northumbria University NEWCASTLE

CUSTOMER SERVICE EXCELLENCE CSE

UniversityLibrary

Check for updates

JGR Space Physics

RESEARCH ARTICLE
10.1029/2020JA028753

Vortex Generation and Auroral Response to a Solar Wind Dynamic Pressure Increase: Event Analyses

Jinyan Zhao[1], Quanqi Shi[1], Anmin Tian[1], Xiao-Chen Shen[2], James M. Weygand[3], Huizi Wang[1], Shutao Yao[1], Xiao Ma[1], Alexander William Degeling[1], I. Jonathan Rae[1,4], Hui Zhang[5], Xiao-Jia Zhang[3], Shi-Chen Bai[1], Wensai Shang[1], and Jong-Sun Park[1]

[1]Shandong Key Laboratory of Optical Astronomy and Solar-Terrestrial Environment, School of Space Science and Physics, Institute of Space Sciences, Shandong University, Weihai, China, [2]Center for Space Physics, Boston University, Boston, MA, USA, [3]Department of Earth, Planetary, and Space Sciences, University of California, Los Angeles, CA, USA, [4]Department of Mathematics, Physics and Electrical Engineering, Northumbria University, Newcastle-upon-Tyne, UK, [5]Geophysical Institute, University of Alaska Fairbanks, Fairbanks, AK, USA

Abstract In this study, we investigate ionospheric responses, including currents and aurorae, to solar wind dynamic pressure (SW P_{dyn}) sudden increases, which are critical for understanding solar wind-magnetosphere-ionosphere coupling. We focus on two similar SW P_{dyn} pulse events that occurred on January 24, 2012 and November 12, 2010. In both cases, equivalent ionospheric currents (EIC) vortices were generated within about 10 min after the pressure pulse arrival, with a counter-clockwise rotating vortex (viewed from above) observed on the dusk side in the former case, and a clockwise vortex observed on the dawn side in the latter. Simultaneous ground-based All-Sky Imager (ASI) observations in the vicinity of the observed EIC vortex in each case showed that aurorae intensified on the dusk side and diminished on the dawn side. These observations provide direct evidence of the scenario proposed by Shi et al. (2014) that magnetospheric flow vortices generated by a solar wind pressure pulse carry field-aligned currents into the ionosphere and thereby modulate auroral activity. The dawn/dusk asymmetry in the auroral intensification is a direct result of the opposite sense of vortex rotation on the dawn and dusk sides, which generate oppositely directed field-aligned currents into/out of the ionosphere.

Plain Language Summary Earth's magnetosphere and ionosphere are strongly affected by variations of the solar wind, especially the variation of solar wind dynamic pressure (SW P_{dyn}). A SW P_{dyn} increase/decrease leads to the compression/expansion of the Earth's magnetosphere. In response, field-aligned currents, which are carried by precipitating or escaping plasma particles, are generated in the magnetosphere, and in turn lead to variations in the auroral intensity. In previous studies of events with similar variations of SW P_{dyn}, cases of both auroral brightening and dimming have been observed. Therefore, it has not been clear whether the aurorae become darker or brighter after SW P_{dyn} increase/decrease events. In this article, we clarify the relationship between the auroral intensity variation and positive SW P_{dyn} pulses. We show that auroral brightening on the dusk side and dimming on dawn side during SW P_{dyn} increase events are due to oppositely directed field-aligned currents in these regions. These are generated by oppositely rotating flow vortices on the dusk and dawn flanks of the magnetosphere, which are both produced by the passage of the SW P_{dyn} pulse.

Key Points:

- Aurora and vortex on dawn/dusk side in response to a positive solar wind dynamic pressure (SW P_{dyn}) pulse are reported
- Positive SW P_{dyn} pulses generate current vortices with an opposite direction on the dawn and dusk side ionosphere, respectively
- Aurorae dimmed/brightened after the appearance of the clockwise/counterclockwise current vortices

Supporting Information:

- Supporting Information S1

Correspondence to:
Q. Q. Shi,
sqq@sdu.edu.cn

Citation:
Zhao, J., Shi, Q., Tian, A., Shen, X.-C., Weygand, J. M., Wang, H., et al. (2021). Vortex generation and auroral response to a solar wind dynamic pressure increase: Event analyses. *Journal of Geophysical Research: Space Physics*, *126*, e2020JA028753. https://doi.org/10.1029/2020JA028753

Received 2 OCT 2020
Accepted 6 FEB 2021

© 2021. American Geophysical Union. All Rights Reserved.

1. Introduction

Positive solar wind dynamic pressure (SW P_{dyn}) pulse events, some originate from various solar wind structures, including the leading edge of HPS (Heliospheric Plasma Sheet; e.g., Shi, Hartinger, et al., 2013; Winterhalter et al., 1994), CIR (Corotating Interaction Region; e.g., Olmsted & Akasofu, 1986) or Coronal Mass Ejection (CME; e.g., Marcia & Raymond, 1997). These can cause the compression of Earth's magnetosphere after their arrival (e.g., Li et al., 2011, 2017, 2008; Shi, Zong, et al., 2013, 2014, 2020, 2009; Russell et al., 2000, 1999; Wilken et al., 1982; Zong et al., 2004). Negative SW P_{dyn} pulse events, originate from the trailing edge of Heliospheric Plasma Sheet (e.g., Winterhalter et al., 1994), Corotating Interaction Region (e.g., Gibson et al., 2009), or the leading edge of magnetic clouds (e.g., Takeuchi et al., 2002), and can cause the expansion of Earth's magnetosphere (e.g., Li et al., 2008, 2011, 2017; Shi et al., 2014, 2020).

Extensive studies have shown that SW P_{dyn} pulses can significantly impact the magnetosphere and the ionosphere. When SW P_{dyn} pulses arrive at Earth's magnetosphere, a single plasma vortex or a pair of plasma vortices appear both on the dawn side and dusk side of the magnetospheric equatorial plane (Birn et al., 2004; Glassmeier et al., 1989, 1992; Keiling et al., 2009; Samsonov et al., 2010; Samsonov & Sibeck, 2013; Shi et al., 2014, 2020; Sibeck, 1990; Sun et al., 2015; Tian et al., 2016; Wang et al., 2010; Wang et al., 2010, 2010). The rotation sense of these vortices are oppositely directed for positive and negative SW P_{dyn} pulses (Shi et al., 2020). The magnetic field lines are distorted by these magnetospheric plasma vortices whereupon field-aligned currents (FACs), connected to ionospheric current vortices, are generated (e.g., Birn et al., 2004; Keiling et al., 2009). Tian et al. (2016) reported a case study of an ionospheric traveling convection vortex (TCV) generated by a SW P_{dyn} pulse. They proposed that the TCV is connected to the simultaneous magnetospheric plasma vortex near the equatorial plane through FACs. Therefore, there is a link among the SW P_{dyn} pulse, FACs, magnetospheric vortices, and ionospheric vortices.

Previous studies have also shown that the SW P_{dyn} pulse can affect auroral activity (e.g., Meurant et al., 2004, 2003; Zhou et al., 2003; Zhou et al., 2012; Zhou & Tsurutani, 1999, 2001) through FACs and plasma vortices in the magnetosphere (e.g., Keiling et al., 2009; Lui et al., 2010; Shi et al., 2020; Tian et al., 2016; Yao et al., 2012). A positive/negative geomagnetic sudden impulse could be generated (Akasofu, 1964; Araki & Nagano, 1988; Takeuchi et al., 2002; Vorobjev et al., 1974), with potential Space Weather consequences for ground-based networks (Carter et al., 2015; Fiori et al., 2014; Marshall et al., 2012; Smith et al., 2019). If the SW P_{dyn} produces a positive/negative sudden impulse, a positive/negative sudden impulse in terrestrial magnetic field can be generated, in addition to magnetospheric compression/expansion at higher altitude (Akasofu, 1964; Araki & Nagano, 1988; Takeuchi et al., 2002; Vorobjev et al., 1974). However, after SW P_{dyn} increase, both an increase (Sato et al., 2001) and decrease (Liou et al., 2006, 2007) of the auroral brightness have been observed. Similarly, many studies have found an enhancement (Hubert et al., 2003; Zhou et al., 2003) and reduction (Zong et al., 2009, 2010) of auroral brightness after SW P_{dyn} increase events. While explanations of the physical mechanisms causing variations in each case were offered, such as FACs (Sato et al., 2001), the loss cone of trapped particles, and the magnetic mirror ratio (Liou et al., 2006, 2007; Hubert et al., 2003; Zhou et al., 2003; Zong et al., 2008, 2009, 2010), none of these provide a convincing, consistent scenario to explain the different variations of auroral brightness under similar conditions of geomagnetic activity during the SW P_{dyn} pulse events.

Shi et al. (2014) first proposed a scenario that attempts to explain observed variations in auroral brightness following the arrival of a positive SW P_{dyn} pulse, whereby this positive pulse can generate FAC in the correct sense to add to or reduce the auroral intensity. The global response after the arrival of a negative SW P_{dyn} pulse (Zhao et al., 2016) can also be explained by this scenario. Here, we introduce the whole scenario in detail. A positive SW P_{dyn} pulse launches compressional waves from the dayside magnetopause into the magnetosphere. These compressional waves propagate into the inner magnetosphere before being reflected toward the morning or afternoon flanks, due to inhomogeneities in the magnetic field as well as cold plasma density (and hence the Alfvén speed) (Allan & Poulter, 1992; Degeling et al., 2014, 2018; Samsonov et al., 2007, Samsonov & Sibeck, 2013; Shi et al., 2014; Yang et al., 2010; Zhao et al., 2016). At the leading edge of the compressional wave/reflected compressional wave as it propagates antisunward down the dawn and dusk flanks, plasma will be accelerated by an Ampere force and move Earthward and Sunward (Samsonov & Sibeck, 2013; Shi et al., 2014; Tian et al., 2016; Zhang et al., 2010; Zhao et al., 2016; Zong et al., 2012). Accordingly, the appearance of a magnetospheric flow vortex can be expected because flow shear is set up at the leading edge of the pressure pulse as it travels down the magnetopause flank. These clockwise or counterclockwise magnetospheric vortices viewed from above the equatorial plane are associated with FACs (Keiling et al., 2009; Shi et al., 2014, 2020; Tian et al., 2016) and generate the clockwise or counterclockwise ionospheric current vortices in the ionosphere (Shi et al., 2014, 2020; Zhao et al., 2016, 2019). The plasma vortices have opposite directions on the dawn and dusk sides both in the magnetosphere and ionosphere because of mirror symmetry in the magnetospheric configuration and compressional wave driver across the noon/midnight meridian. The rotation direction of the ionospheric plasma vortex is clockwise on the dusk side and counterclockwise on the dawn side, when looking down at the Northern hemisphere from above the Earth. Figure 1 clearly shows the schematic of the whole process of the magnetosphere and ionosphere to a SW P_{dyn} impulse. The curved green arrows indicate the direction of the FACs. The FACs, carried by escaping electrons on the dawn side and precipitating electrons on the dusk side, are downward and upward

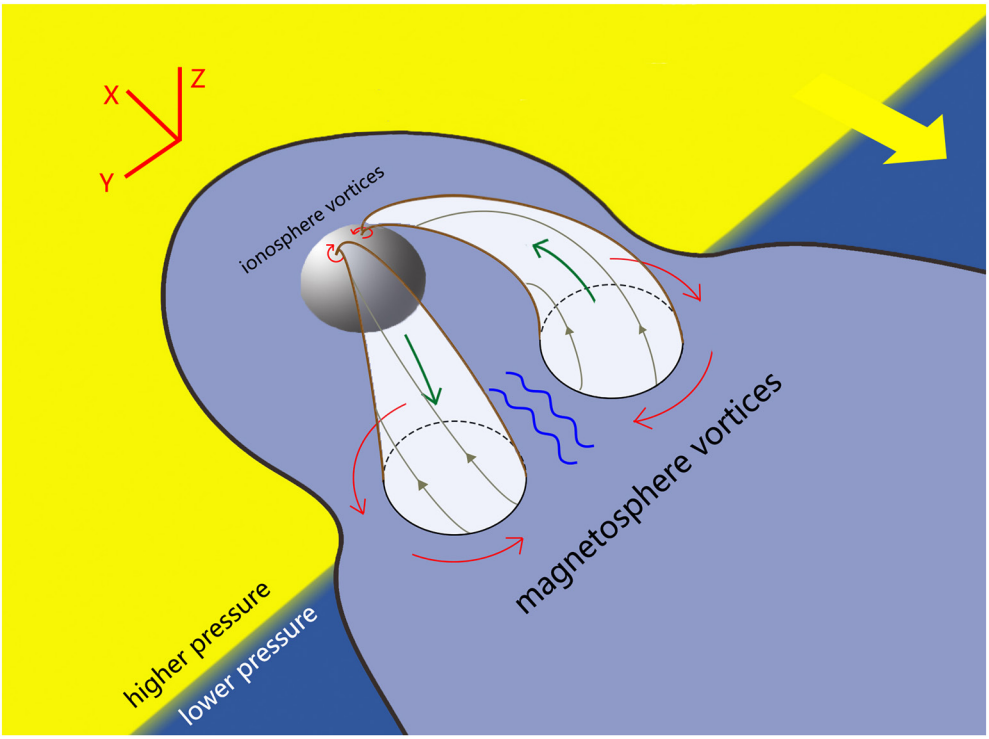

Figure 1. Schematic view of some responses in the Earth's magnetosphere and ionosphere to a positive SW P_{dyn} pulse (from Shi et al., 2020). Red arrows indicate the sense of vortex rotation in the equatorial plane and ionosphere, and green arrows indicate the direction of filed-aligned current within the vortex magnetic flux tubes, which act to locally twist magnetic field lines (gray lines). SW P_{dyn}, solar wind dynamic pressure.

on those two flanks respectively. Therefore, aurora close to the ionospheric current vortex in the dawn/dusk side will become dimmer/brighter, respectively.

In previous studies, part of the scenario mentioned above (the magnetospheric plasma vortex generated by SW P_{dyn} pulse) has been verified in simulation method (e.g., Tian et al., 2016; Zhao et al., 2016). Nevertheless, due to the absence of conjugate auroral observations, the entire chain of the response has not been demonstrated. Fortunately, on account of requisite parameters of solar wind and magnetosphere in situ observations, and aurora observation on the dawn and dusk sides, we are able to verify the whole scenario carefully for the first time in this article.

The detailed observations of our events are shown in Section 2. The case of a dusk side event is shown in Section 2.1, and the dawn side event is shown in Section 2.2, followed by the summary and discussion in Section 3.

2. Northern Hemispheric Vortex and Aurora Responses to a Positive Pressure Pulse

In this section, we present two events in which a positive SW P_{dyn} pulse impacted the magnetosphere, and show: (i) the evolution of equivalent ionospheric current (EIC) vortices, (ii) the generation of FACs, and (iii) their effect on auroral activity in the corresponding EIC vortex region; on the dusk (Section 2.1) and dawn side (Section 2.2), respectively. In so doing, we demonstrate the causal chain of processes between the positive SW P_{dyn} pulse, EICs vortices, FACs, and changes in auroral intensity.

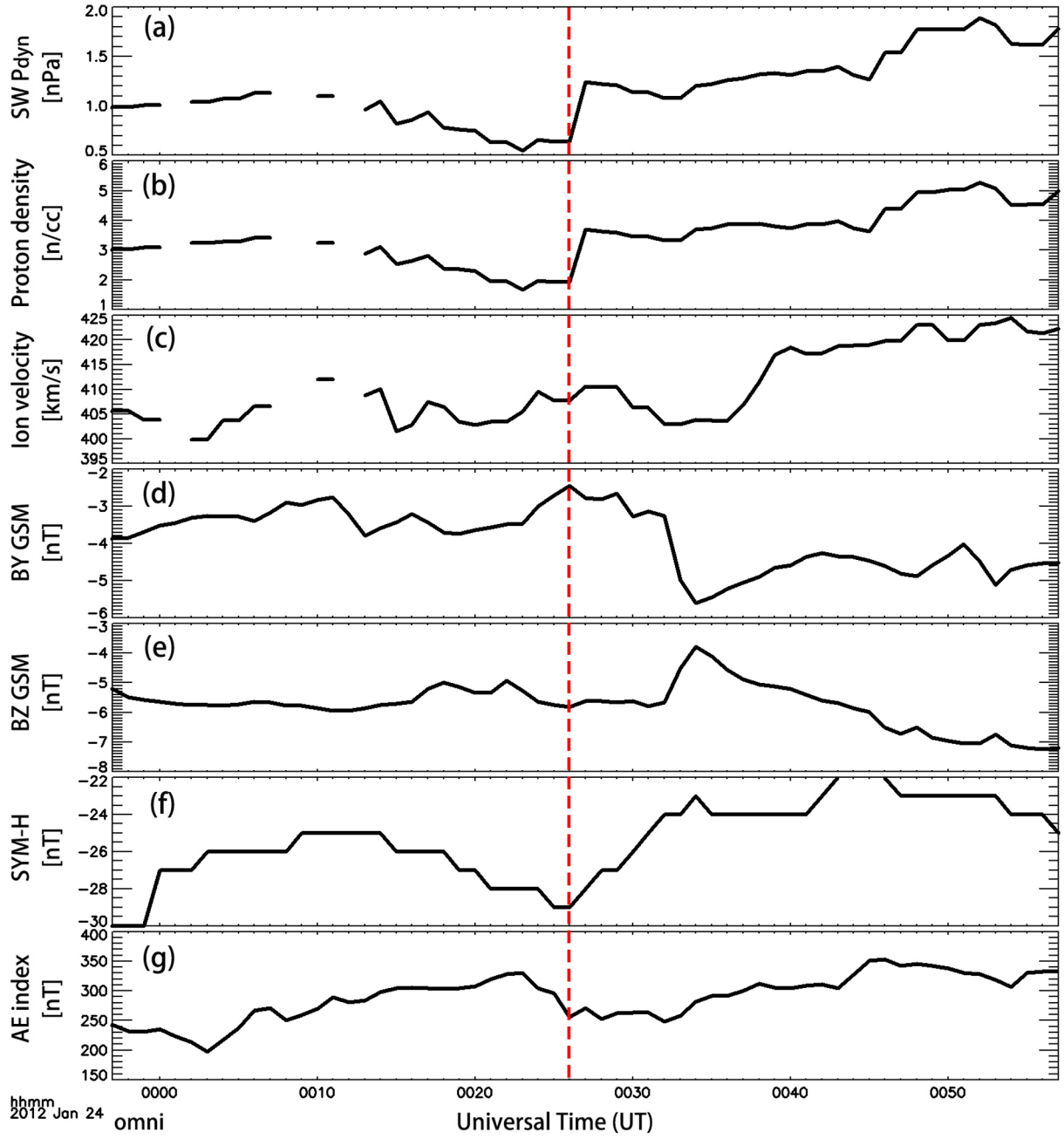

Figure 2. Solar wind, IMF, and geomagnetic conditions during 00:00-01:00 UT on January 24, 2012 from OMNI data set. (a) SW P_{dyn}, (b) proton density, (c) ion velocity, (d) IMF B_y, (e) IMF B_z, (f) SYM-H, and (g) AE index. The red vertical dashed line shows the arrival time of positive SW P_{dyn} pulse. IMF, interplanetary magnetic field; SW P_{dyn}, solar wind dynamic pressure.

2.1. Dusk Side Counterclockwise Vortex Generation and Aurora Intensity Increases

The solar wind and the interplanetary magnetic field (IMF) measurements during 00:00–00:50 UT on January 24, 2012 from the OMNI database are shown in Figure 2. We note that the IMF data are displayed in the Geocentric Solar Magnetospheric (GSM) coordinate system. As shown in Figure 2a, the SW P_{dyn} increases from ~0.6 to 1.2 nPa at ~00:26 UT (red vertical dashed line) within 2 min, which is mainly due to an abrupt increase in proton density (as shown in Figure 2b). Figures 2d and 2e show that during 00:00–01:00 UT, the IMF B_y decreases from −3 to −5 nT, while the IMF B_z increases from −6 to −4 nT. The increase of SYM-H, from 00:26 to 00:34 UT as shown in Figure 2f, indicates a compression of the magnetosphere by the positive

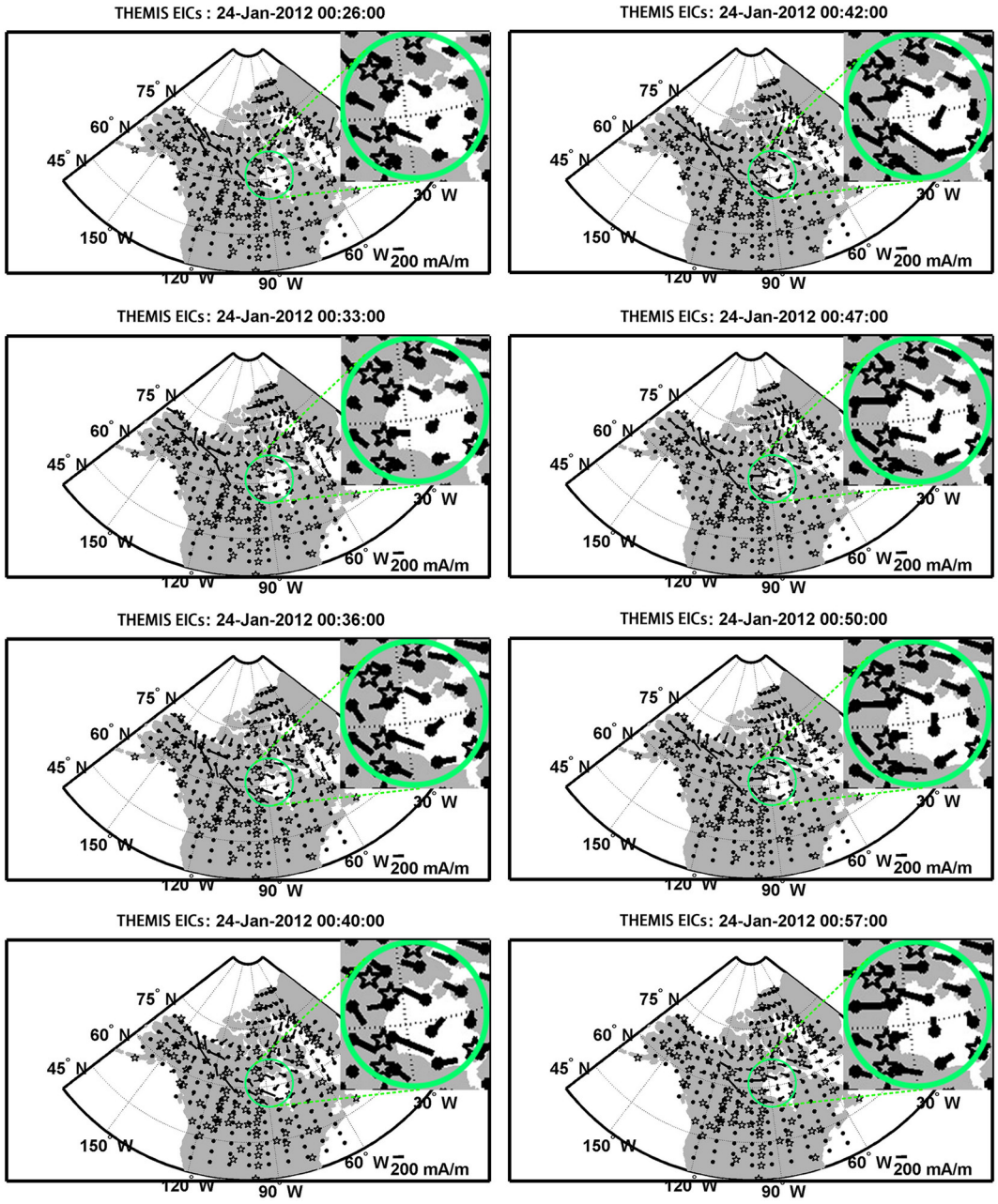

Figure 3. Panels from top to bottom and left to right show the spatial distributions of the equivalent ionospheric currents (EICs) at each moment from 00:26 UT to 00:57 UT on January 24, 2012. The black dots mark the computational grid for the elementary currents. Short black lines indicate the magnitude and direction of equivalent ionospheric currents. The EICs vortex is marked as green circle, and a zoomed-in view is shown in the upper right corner of each panel. EIC, equivalent ionospheric currents.

SW P_{dyn} pulse, which can be used to determine the arrival time of the pressure pulse. In Figure 2g, the small-to-moderate AE index (~280 nT) have a minimal variation during the time period of observation.

In order to demonstrate the relation between the EICs vortex and the SW P_{dyn} increase, we show the evolution of the EICs vortex, derived from THEMIS/CARISMA/BLC (Mann et al., 2008; Newitt et al., 2007; Russell et al., 2008) ground-based magnetometer observations, with universal time in Figure 3. An EICs vortex, obtained by taking ionospheric currents data from the ground magnetometer arrays and using the Spherical Elementary Currents (SECs) method (e.g., Amm, 1997; Amm & Viljanen, 1999; Weygand et al., 2009b,

2011), whose direction of rotation is counterclockwise with a scale size (diameter) of about 400 km, is generated at 00:33 UT (18:33 LT) on January 24, 2012.

Here, we briefly describe the computing methods in Amm (1997) for obtaining EIC. This method expands the ionospheric currents system (assuming that the field-aligned currents flow radially) based on two sets of basis functions described in spherical coordinates. One of these basis functions is curl-free and poloidal which can cause a toroidal magnetic field confined above the ionosphere, and the other function is divergence-free and toroidal, which can cause a poloidal magnetic field below the ionosphere, resulting from ionospheric currents. These basis functions comprise the Spherical Elementary Currents (SECs) mentioned above with, the equivalent ionospheric current (EIC) equal to the sum of divergence free parts of the Hall and Pedersen currents.

Figure 3 shows the details of an EIC vortex, with each panel displaying a snap-shot of the spatial distribution of EICs at the indicated time, in which black vectors indicate the magnitude and direction of the ionospheric current. The green circle indicates the scope of the EICs vortex. In order to make a distinct comparison easier a magnified view of the EICs vortex is provided in the upper right corner of each panel, which appears to be centered close to the East coast of the Hudson Bay inlet in Northern Canada. In Figure 3, from 00:26 UT to 00:32 UT, the magnitude of currents are exceedingly small in this region and have not formed a clear vortex profile. A single counterclockwise current vortex with relatively small current magnitude less than ~200 mA/m is apparent at 00:33 UT (18:33 LT). The current magnitude at all directions in vortex increase slightly from 00:33 UT (18:33 LT) and decrease from 00:50 UT (18:50 LT). The geographic location of this flow vortex, around at (60°N, 90°W), remains unchanged for 24 min.

Previous research has shown that counterclockwise/clockwise vortices in equivalent ionospheric currents are associated with upward/downward field-aligned currents (e.g., Fukushima, 1976; Shi et al., 2020; Tian et al., 2016; Zhao et al., 2019). We used the method of Zhao et al. (2019) to estimate the distribution of FACs from the computed EICs during this event. This method assumes that gradients in the ionospheric conductance perpendicular to the direction of the electric field are negligible, in which case it can be shown that the Hall-to-Pederson conductance ratio (known as the SEC system factor, and given by integrating the vertical component of the curl of EIC over each grid cell) is proportional to the local field-aligned current density (Amm & Kauristie, 2002; Weygand et al., 2011, 2016). Only regions above 38° geographic latitude are considered in this method, in order to restrict the calculation to regions where the vertical direction approximately corresponds to the field-aligned direction (e.g., Amm, 1998; Amm & Kauristie, 2002; Weygand et al., 2011, 2009; Zhao et al., 2019). The resultant SECs amplitudes, which are proportional to the FACs for our event are displayed in Figure 4. The upward/downward currents are indicated by red plus symbols/blue squares, respectively, with a symbol size that is proportional to the current magnitude. In order to investigate the relationship between the variation of auroral intensity with the EIC vortex and FAC distribution, we first mark the field-of-view of the All-Sky Imager (ASI) for auroral observations at the GILL ground station (using a yellow circle in Figure 4), and use a green circle (similarly marked in Figure 3) to indicate the vicinity of the vortex. We also provide in Figure 4 magnified views of the SECs amplitude distribution at the location of the vortex and the ASI GILL ground station in the upper right corner of each panel. Comparing Figures 3 and 4, we find that the core of the vortex is situated in a region of upward currents, and that part of this region lies within the ASI field of view of the GILL ground station.

In Figure 5a, we calculated the sum of the upward and downward currents in the field-of-view of ASI GILL ground station (the yellow circle area as shown in Figure 4). The red/blue histograms show the sum of upward/downward currents in the ASI GILL ground station field of view at each moment, with 10 s time resolution. The vertical black line indicates the time at which upward currents start to increase. The upward currents increase slowly from 00:37 UT and reach the maximum value at ~01:00 UT, while the downward currents increase rapidly from 00:34 UT to 00:37 UT and decrease slowly from 00:37 UT to 01:00 UT. To check which type (upward/downward) of currents dominate the region in the scope of ASI GILL ground station over time, we show the total current amplitudes for every 10 s in Figure 5b, which is the difference between the upward and downward currents. The vertical black line marks the start time at which the FACs are dominated by upward currents in the above region. Figure 5b clearly shows that the FACs in the area of ASI GILL observation are mainly upward from 00:45 UT to 01:00 UT, and the upward currents gradually increase compared with the downward currents. This situation is consistent with the upward FACs (the

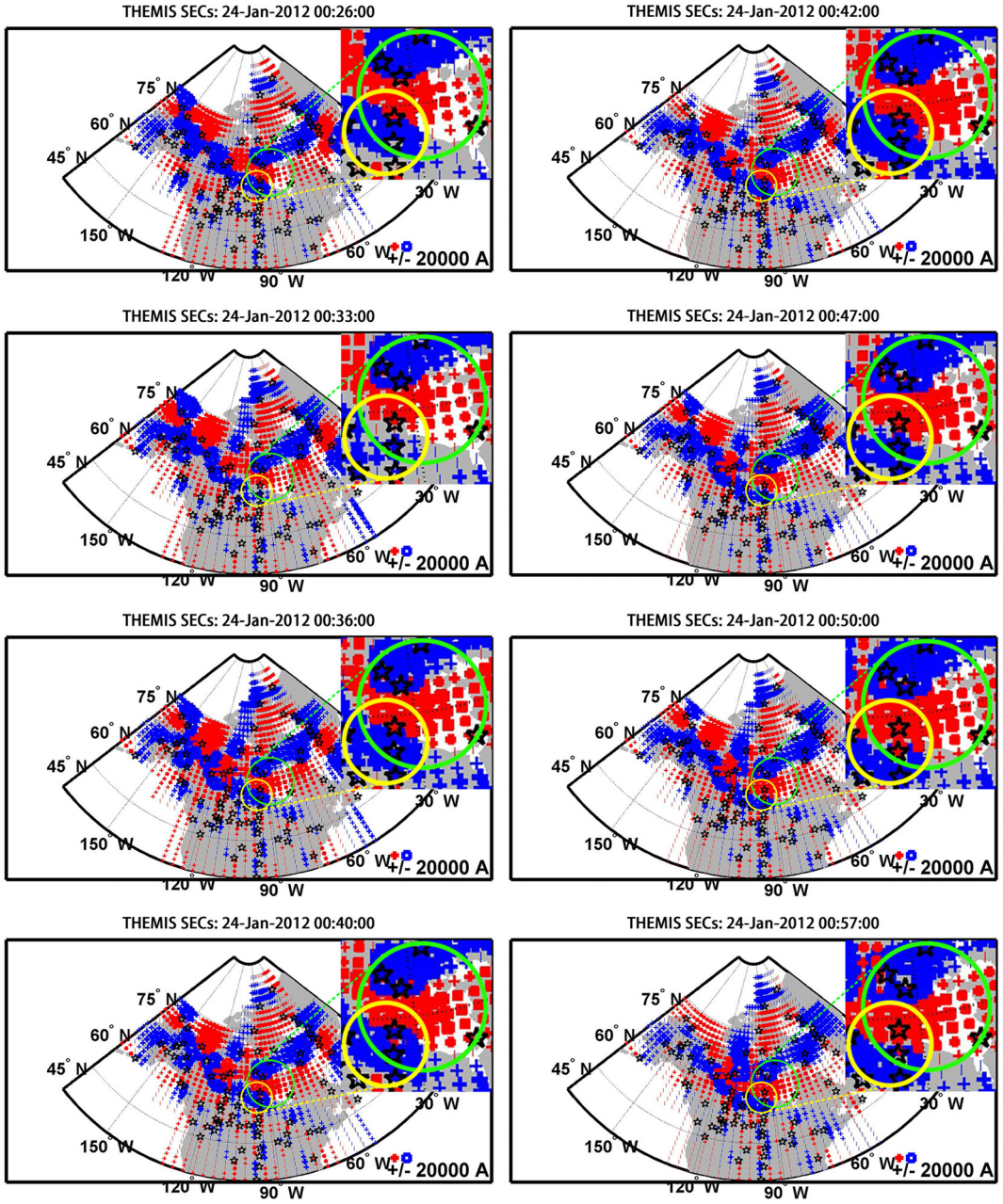

Figure 4. Upward (red "+" symbols) and downward (blue squares) currents estimated using the SECs model over North America, at various times from 00:26 UT to 00:57 UT on January 24, 2012 are shown in the same order as Figure 3. The current magnitude is indicated by the symbol size. The yellow circle indicates the Field-of-View of the All-Sky Imager (ASI) GILL ground station. The green circle marks the vortex position (as similarly marked in Figure 3). ASI, All-Sky Imager.

curved green arrow) on the dusk side in Figure 1. Because the FACs are carried by ascending and precipitating electrons which could affect auroral activities (e.g., Lyons et al., 1986; Rostoker et al., 1985), a strong enhancement of auroral intensity should be observed from ~00:37 UT (18:37 LT) onwards, associated with the red plus symbols inside the yellow circle at GILL ground station in Figure 4.

Therefore, the ASI aurora observations at GILL ground station are necessary to verify this point. We used false chromatic color to clearly show the variation of auroral brightness, as shown in Figure 6. To more accurately quantify the auroral intensity variation, we selected five different vertical slices to display keograms,

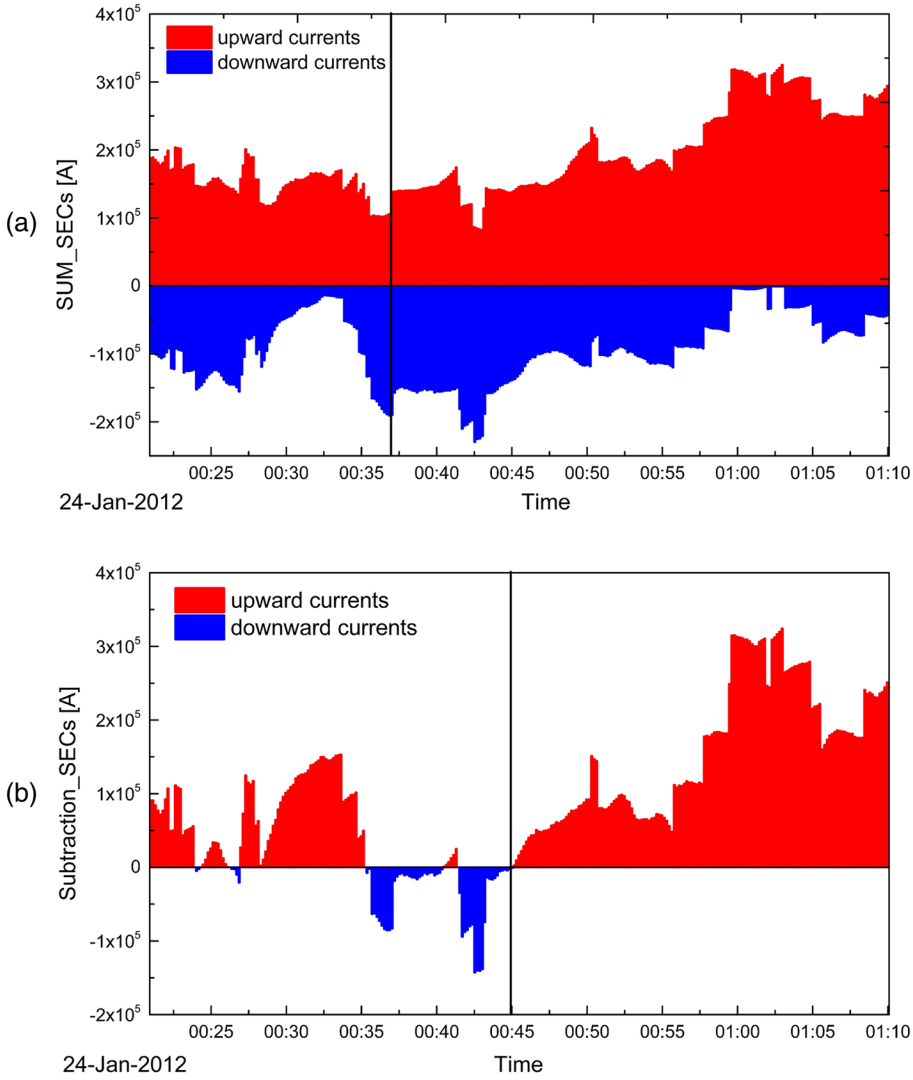

Figure 5. (a) The sum of upward currents (red bars)/downward currents (blue bars) within the Field-of-View of the GILL ground station All-Sky Imager (yellow circle in Figure 4). (b) The differences between the upward currents and downward currents. The vertical black line in (a) indicates the time (00:37 UT) currents start to increase in the above region and in (b) indicates the start time when the FACs, in the region of GILL ASI observations, are dominated by upward currents (00:45 UT). ASI, All-Sky Imager.

shown in Figures 7a–7e. We also selected a region from the GILL station observations with strong upward currents (observed in Figure 4) and clear aurora (observed in Figure 6) to plot the average aurora intensity as shown in Figure 7f. The positions of these selected slices and auroral area are marked by red vertical lines (a)~(e) and a red box (f) in Figure 6, respectively. The auroral intensity slowly increases from 00:34 UT (18:34 LT) and obviously increases from 00:37 UT (18:37 LT) as expected, which is consistent with the arrival time of the positive SW P_{dyn} pulse (at 00:26 UT as shown in Figure 2a) and the higher SYM-H index (from 00:26 to 00:34 UT as shown in Figure 2f), the generation time of the ionospheric EICs vortex (at 00:33 UT as shown in Figure 3), and the situation of upward FACs distribution (increases slowly from 00:37 UT as shown in Figure 5a) in ionosphere.

In summary, we find that a counterclockwise EICs vortex in the dusk side is generated in the ionosphere within 10 min after the arrival of positive SW P_{dyn} pulse. Upward FACs increase at the same location after the formation of the EICs vortex. There is a clear relation between the enhancement of upward FACs and auroral brightness at the same location in the dusk side. These observations demonstrate the chain reaction

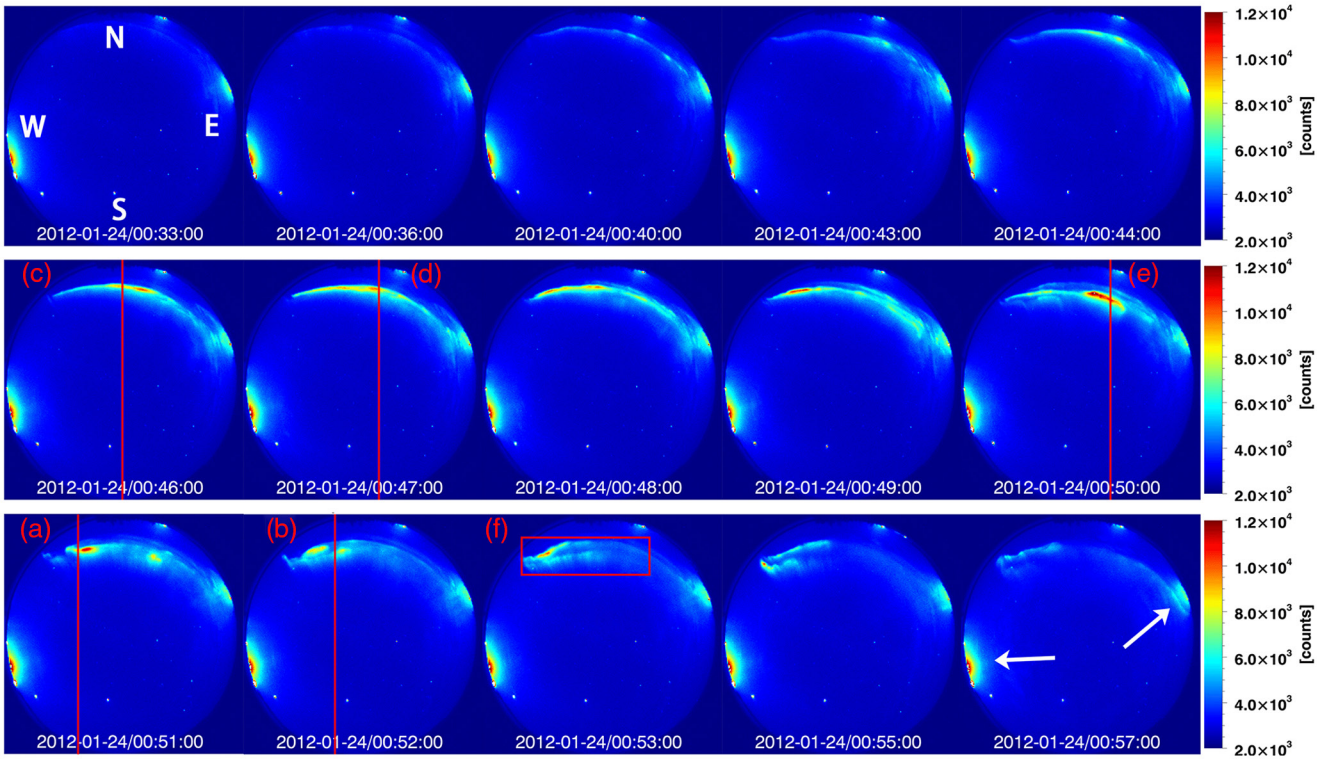

Figure 6. From left to right, top to bottom show false-color Auroral images at ASI GILL station from 00:33 UT to 00:57 UT on January 24, 2012. The vertical red lines ((a)–(e)) are the locations of auroral slices selected for Figure 7. The red box (f) is a region chosen for calculating the average value of auroral intensity. The white arrows indicate light pollution (the moon on the left and the reflection of the moon on the right side). ASI, All-Sky Imager.

on the Earth's dusk side between the positive SW P_{dyn} pulse, counterclockwise EICs vortex in the ionosphere, upward FACs, and the enhancement of auroral intensity.

2.2. Dawn Side Clockwise Vortex Generation and Aurora Intensity Decreases

The second case of our study, which occurred on November 12, 2010, was triggered by the arrival of a SW P_{dyn} pulse at 10:46 UT, with similar characteristics to pulse in the first case described in Section 2.1. In this case, however, a clockwise vortex (viewed from above) and weakening aurora are recorded on the dawn side of Earth's ionosphere. The rotation sense of the vortex and auroral intensity variation are opposite to those in the previous case. We follow the same steps described in the above section to study this case.

Figure 8 shows the time-variation of solar wind parameters and the SYM-H index during the interval of interest. The red vertical dashed line indicates the moment just prior to the SW P_{dyn} increase, at 10:46 UT. The pressure changes from ~2.5 to 4.0 nPa within 4 min, which is also mainly due to the variation of proton density (see Figures 8b and 8c). It can be seen from Figures 8d and 8e that both the IMF B_y and the IMF B_z are decreased at the same time and have a reversal from positive to negative at around 10:46 UT. The SYM-H index begins to increase at 10:48 UT and reaches a plateau at 10:52 UT, before increasing further at 10:58 UT. The AE index is less than 250 nT during 10:30–11:10 UT (Figure 8g).

At 10:48 UT, as shown in Figure 9, an EICs vortex with clockwise rotation is generated, shortly after a positive SW P_{dyn} pulse arrived. We show the evolution with universal time of this EICs vortex in Figure 9. The location of the center of the vortex is around at (68°N, 126°W) and the dimension of the vortex is about 400–600 km. During 10:46–10:50 UT (02:46–02:50 LT), the outline of vortex becomes more distinct. After 10:53 UT (02:53 LT), the magnitudes of currents reduce to the minimum. This vortex become less obvious at 11:02 UT (03:02 LT).

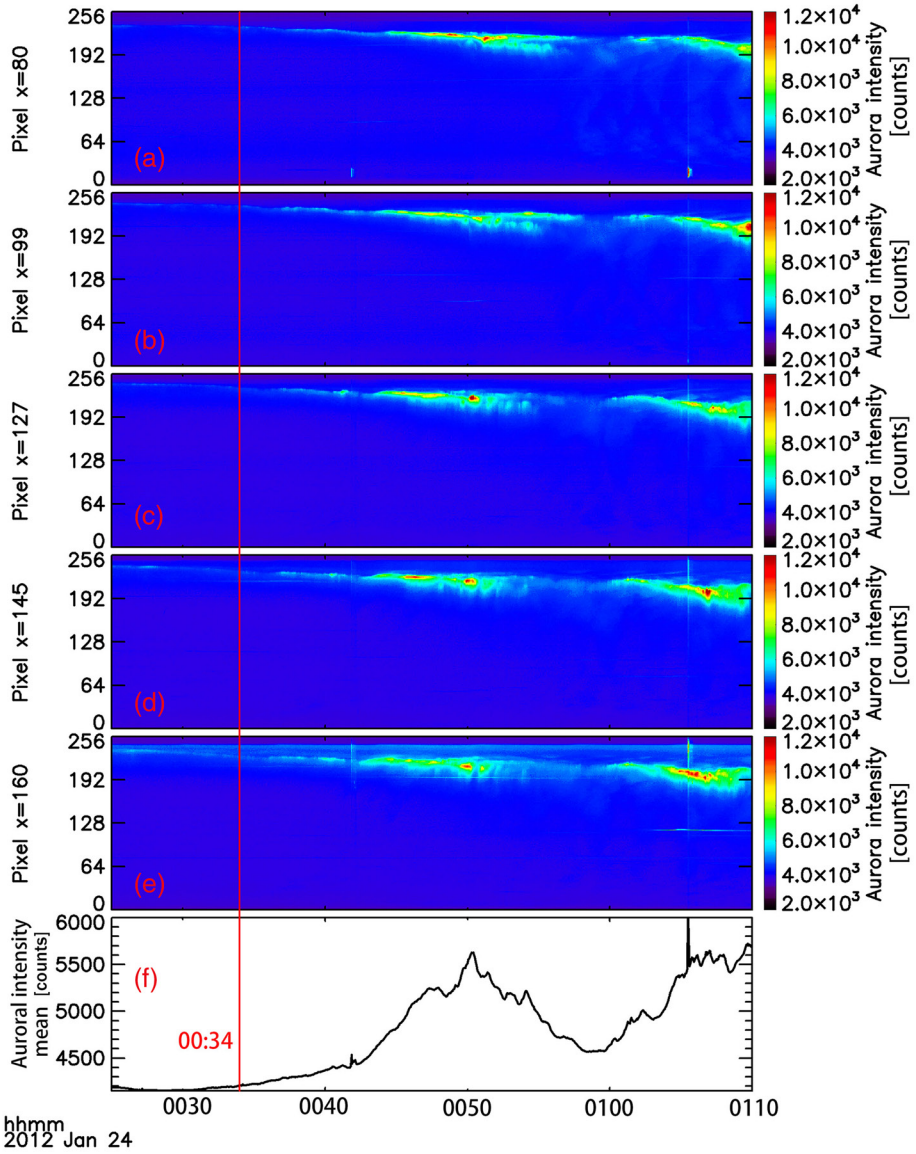

Figure 7. ((a)–(e)): Time variation of auroral intensity along slices ((a)–(e)) taken from Figure 6 (from 00:25 to 01:10 UT). The bottom panel (f) shows the time variation of the average value of auroral intensity within the red rectangle in Figure 6. The red perpendicular at 00:34 UT indicates the beginning time of increased auroral intensity.

We show the SECs amplitudes distribution of this dawn side event in Figure 10, in which the red plus symbols/blue squares correspond with upward/downward currents, similar to Figure 4. The green circle indicates the vicinity of the vortex (as similarly marked in Figure 9) and the yellow circle indicates a location where ASI aurora observations were taken at INUV ground station. Histograms of the upward and downward directed currents (summed over the ASI field of view) are shown as a function of time with 10 s resolution in Figures 11a. The vertical black line in this plot indicates the approximate time where both upward and downward currents begin to decrease. The sum of upward currents decreases from 10:48 UT to 10:53 UT (02:48 LT to 02:53 LT), suggesting that the flux of precipitating electrons decreases during this interval. Figures 11b shows the difference between the upward and downward directed currents shown in Figures 11a. This figure shows that after 10:42 UT (the vertical black line in Figures 11b), the FACs within the ASI INUV field of view are mainly dominated by downward currents. The downward currents gradually increase compared with the upward currents in this region, which is also consistent with the scenario shown in Figure 1. There is a lack of the upward FACs (precipitating electrons) in the observation area of

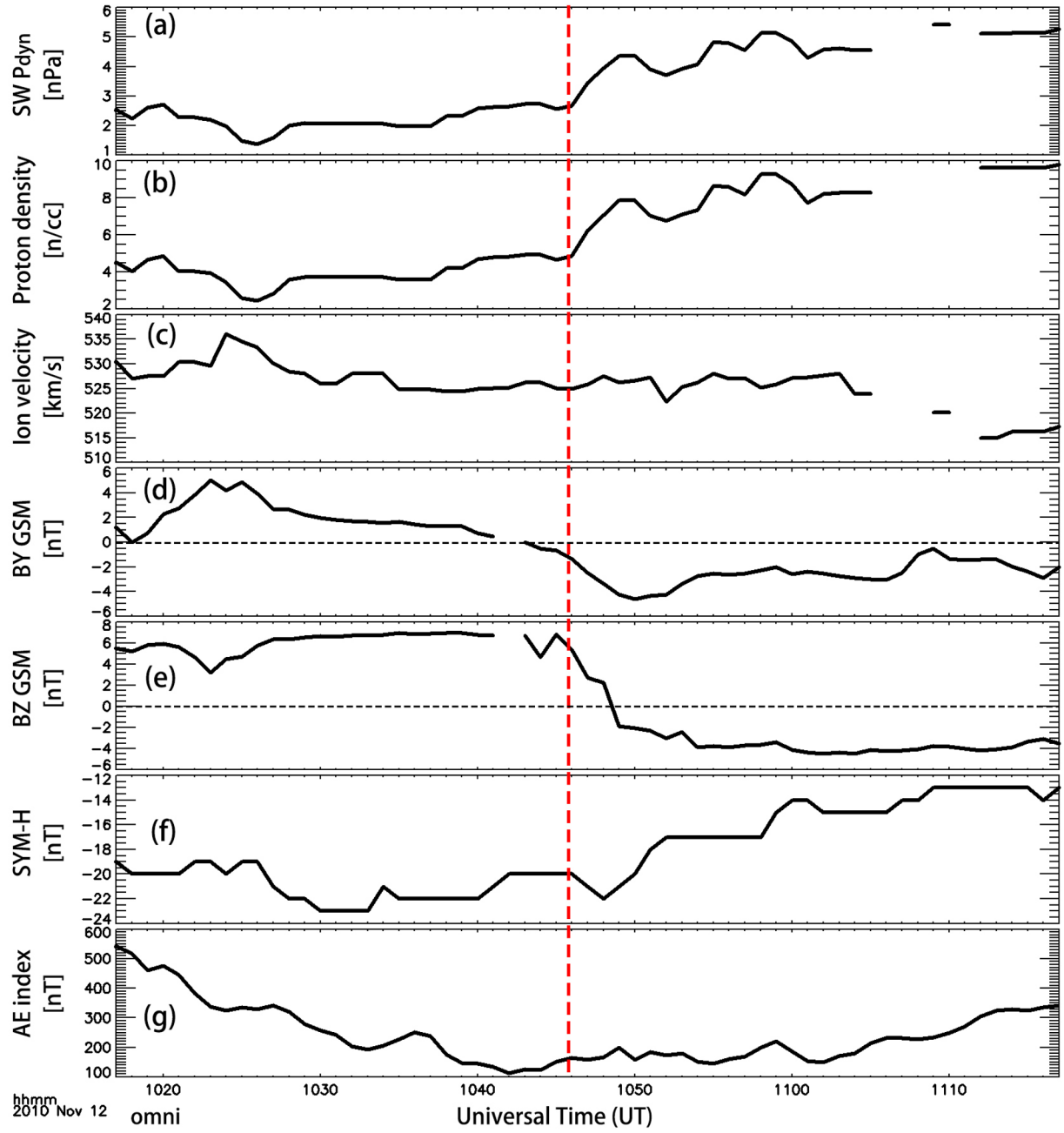

Figure 8. Same as Figure 6, but during 10:20–11:10 UT on November 12, 2010. The dashed red perpendicular shows the arrival time of positive SW P_{dyn} pulse. SW P_{dyn}, solar wind dynamic pressure.

ASI INUV station to maintain the brightness of the aurorae. Therefore, the intensity of aurorae is expected to diminish with time in this region.

The auroral observations at ASI INUV ground station are necessary to verify the above prediction. The same method used to produce Figures 6 and 7 is used to obtain Figures 12 and 13 for this event. We can see the overall variation of auroral intensity with time in Figure 12. The aurora in the region indicated by red arrow 1 diminishes from 10:45 UT (02:45 LT); the aurora in another region indicated by red arrow 2 begins to diminish at 10:48 UT (02:48 LT), and the aurora in the third region indicated by red arrow 3 also begins to diminish at 10:51 UT (02:51 LT). The white arrow indicates light contamination from another light source. We cut five vertical slices (a)~(e) (as marked in Figure 12) in these three auroral regions to track auroral

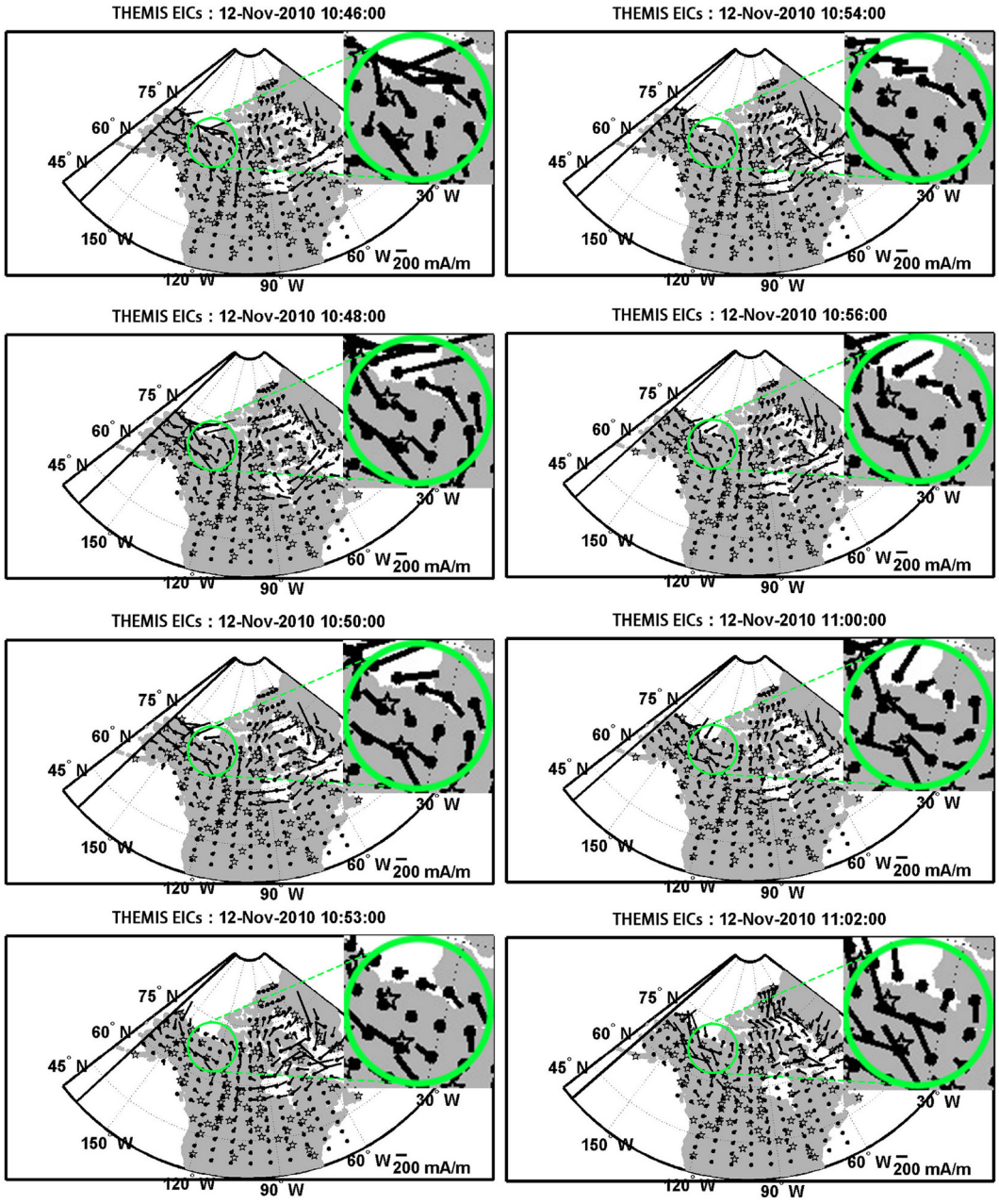

Figure 9. Spatial distributions of the EICs at various times from 10:46 UT to 11:02 UT on November 12, 2010 are shown in the same order as Figure 3. The black line in the north-south direction at about 170° geographic longitude indicates local geographic midnight (Weygand et al., 2009a, 2011). Other parameters are the same as Figure 3. EIC, equivalent ionospheric currents.

intensity variation with time. The details are shown in Figures 13a–13e. The average auroral intensity integrated over the red box (f) (as marked in Figure 12) is shown in Figure 13f, and clearly shows a decrease with time from 10:50 UT (02:50 LT). Finally, all the aurorae in the above three areas are extinguished after 10:50 UT.

Figure 13f shows a sudden drop in intensity between 10:47 and 10:48 UT, which appears to be inconsistent with our predictions from the current amplitude results shown in Figure 11. From Figure 12, we can see from the aurora distribution at 10:47 and 10:48 UT, that the aurora still exists but occupies a very small area close to the left edge of the plot (intersected by line "a"). Therefore, the average value of the auroral intensity

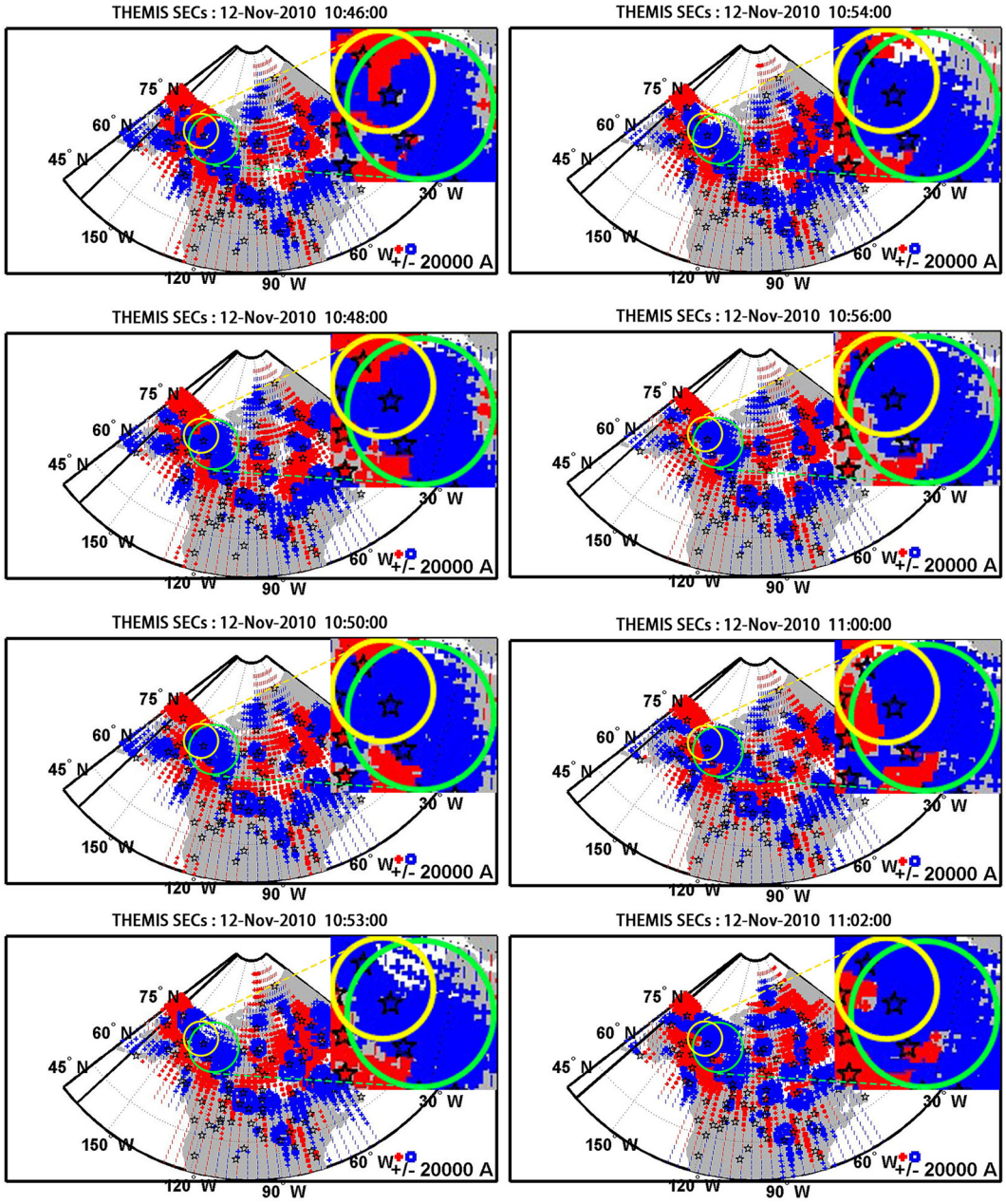

Figure 10. Upward (red "+" symbols) and downward (blue squares) field aligned currents estimated using the SECs model over North America at various times, from 10:44 UT to 11:02 UT on November 12, 2010, are shown in the same order as Figure 4. The current amplitude magnitude is indicated by the symbol size. The yellow circle indicates the location and field of view of the ASI INUV ground station and the green circle indicates the vortex position. The black long line at about 170° of geographic longitude indicates the local geographic midnight (Weygand et al., 2009, 2011) same as Figure 9. ASI, All-Sky Imager.

that we calculated in the region of the red box is relatively small. We can see the variation of auroral intensity on one slice in this small region in Figure 13a.

The characteristics of this event may be summed up as follows: the SW P_{dyn} arrives at the magnetopause at 10:46 UT. After 2 min, a clockwise EICs vortex on the dawn side forms near the INUV ground station, when the SYM-H value begins to increase at 10:48 UT. Downward field-aligned currents associated with the vortex become increasingly dominant within the field of view of an ASI at the station, and the observed auroral intensity diminishes after 10:50 UT. Within the field-of-view of ASI at INUV station, the downward

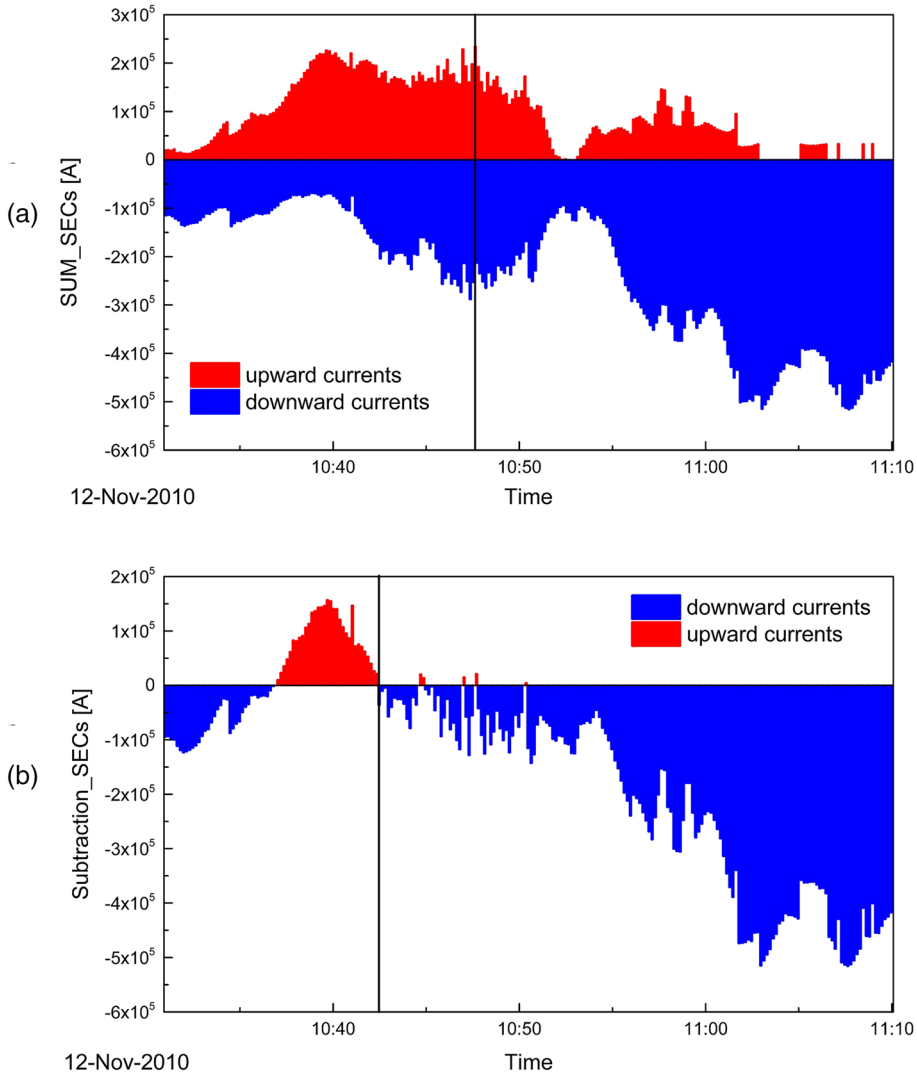

Figure 11. (a) The sum of currents within the field of view of the ASI INUV ground station (yellow circle in Figure 10). (b) The subtraction of upward and downward currents in the above region. The vertical black lines in (a) indicates the time (at 10:47 UT) when currents start to decrease and in (b) indicates the start time (at 10:42 UT) when the FAC, in the region of INUV observation, becomes dominated by downward currents. ASI, All-Sky Imager; FAC, field-aligned currents.

field-aligned currents associated with EIC vortex become increasingly dominant, and the observed auroral intensity here diminishes after 10:50 UT. The current amplitude variation is consistent with the variation of auroral intensity at the same location. The above ionospheric responses in this dawn side event are opposite to the event on the dusk side in Section 2.1.

Our observations provide convincing evidence of a specific chain of coupled processes during SW dynamic pressure pulse events that link the SW P_{dyn} increase, the generation of counterclockwise/clockwise EICs vortices on the dusk/dawn side of the ionosphere, FACs, and the auroral intensity enhancement/weakening on the dusk/dawn side.

There are actually two vortices in Figure 9. A larger scale vortex (60°–75°N, 60°W) shows the opposite direction from the vortex (68°N, 126°W) we discussed above. We use a red dotted line to mark it in Figure 9 to obtain Figure S1 of the supporting material. It is found that this vortex formed at 10:37 UT (~5:37 LT) and disappeared at 11:08 UT (~7:08 LT). This is a traveling vortex on the dawn side, which moves to the southeast from 11:03 UT (as shown in Figure S2). However, a large variation in SW P_{dyn} occurs at 10:46 UT

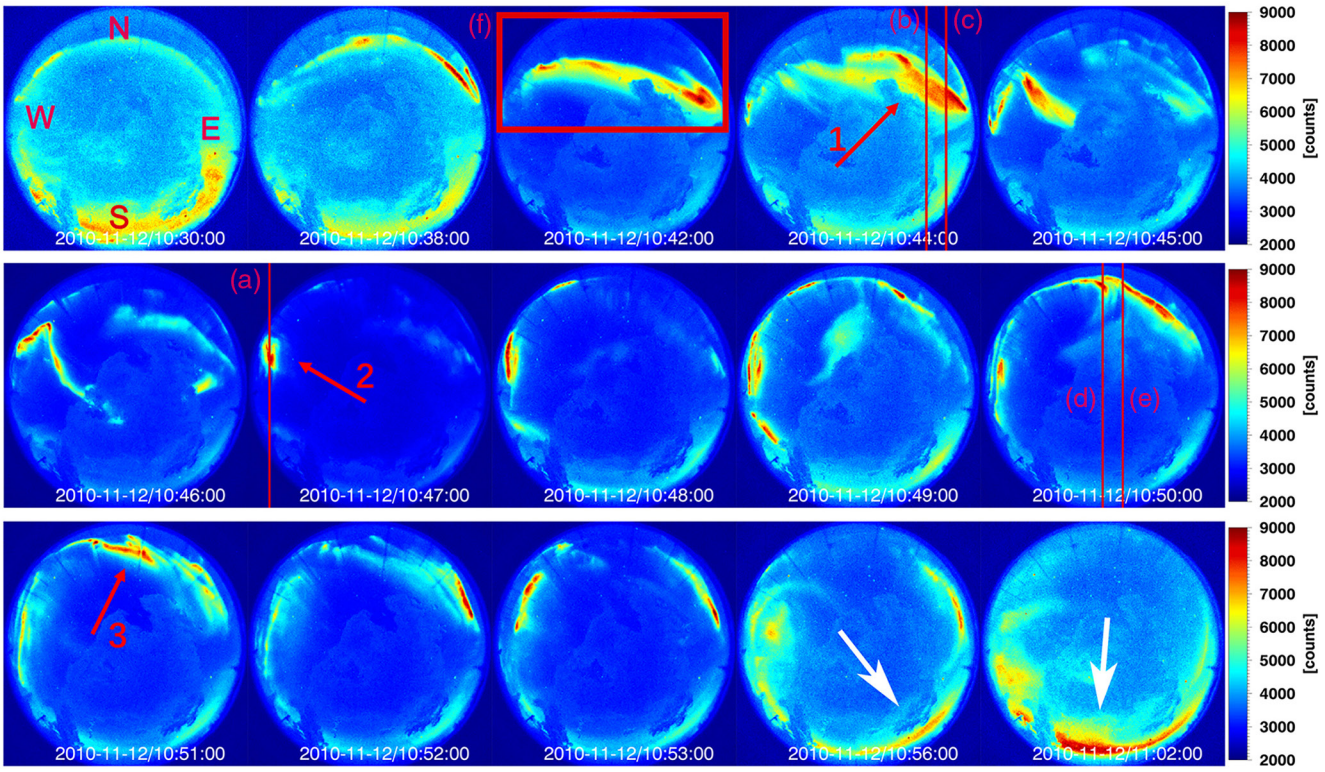

Figure 12. From left to right, top to bottom figures show false-color auroral images taken from the ASI INUV station from 10:30 UT to 11:02 UT on November 12, 2010. The vertical red lines ((a)–(e)) are the locations of selected auroral slices for Figure 13. The red box (f) is a region chosen for calculating the average value of auroral intensity. The red arrows indicate where the aurora is occurring, and the light in the Field-of-View at the edge indicated by the white arrows may be light pollution. ASI, All-Sky Imager.

(as shown in Figure 8a) after the vortex occurs at 10:37 UT. This indicates that there may be no causal relationship between this vortex and SW P_{dyn} variation, or at least that this vortex is not induced by this SW P_{dyn} variation at 10:46 UT. This counter-clockwise vortex on the dawn side is inconsistent with the ideal model proposed by Shi et al. (2020), in which a single antisunward traveling vortex is generated by a SW P_{dyn} pulse. Figure S3 shows the auroral observations between 10:45 UT and 11:02 UT from four ASI ground stations (TALO, RANK, SNKQ, KUUJ) near this vortex. Panels ((a)–(e)) show the distribution of ASI ground stations in North America between 10:45 UT and 11:02 UT. The red dashed line indicates the region where this vortex exists. Regrettably, there are no ASI stations in the central area of this vortex. Only some ASI stations (TALO, RANK, SNKQ, KUUJ) at the edge of the vortex provided observations at that time. Panels ((f)–(i)) show false-color fields of view taken from ASIs at TALO, RANK, SNKQ, KUUJ stations, respectively. These suggest that no aurorae occurred here during the existence of the vortex. These panels show minimal auroral activity within their fields of view over the time interval of interest, however, we cannot definitively determine whether or not this vortex can be associated with an increase in auroral activity because of a lack of auroral observations in the central region of the vortex. Finally, we examine the SECs amplitudes in the central region of the vortex. In Figure S4, the bright blue dashed line indicates the location of the vortex, similar to Figure S1, and the bright blue solid line marks the center of the EIC vortex. Figure S5 calculates the difference between the upward and downward field-aligned currents in the bright blue solid line region. It is found that the central region of this vortex is dominated by upward currents. After the vortex moves southeast at 11:03 UT, the position of the old vortex center is gradually controlled by more powerful downward currents. In addition, we have also found the existence of two adjacent vortices with opposite directions in other events. Actually, there are a number of observations of oppositely directed EIC vortices. Many of these EIC vortices are associated with substorm onset and could very well be linked with convective vortices in the tail on either side of a highspeed earthward flow (e.g., Keiling et al., 2009). Sometimes these EIC vortices are located respectively in the ionospheric flanks (dawn and dusk side), which may be

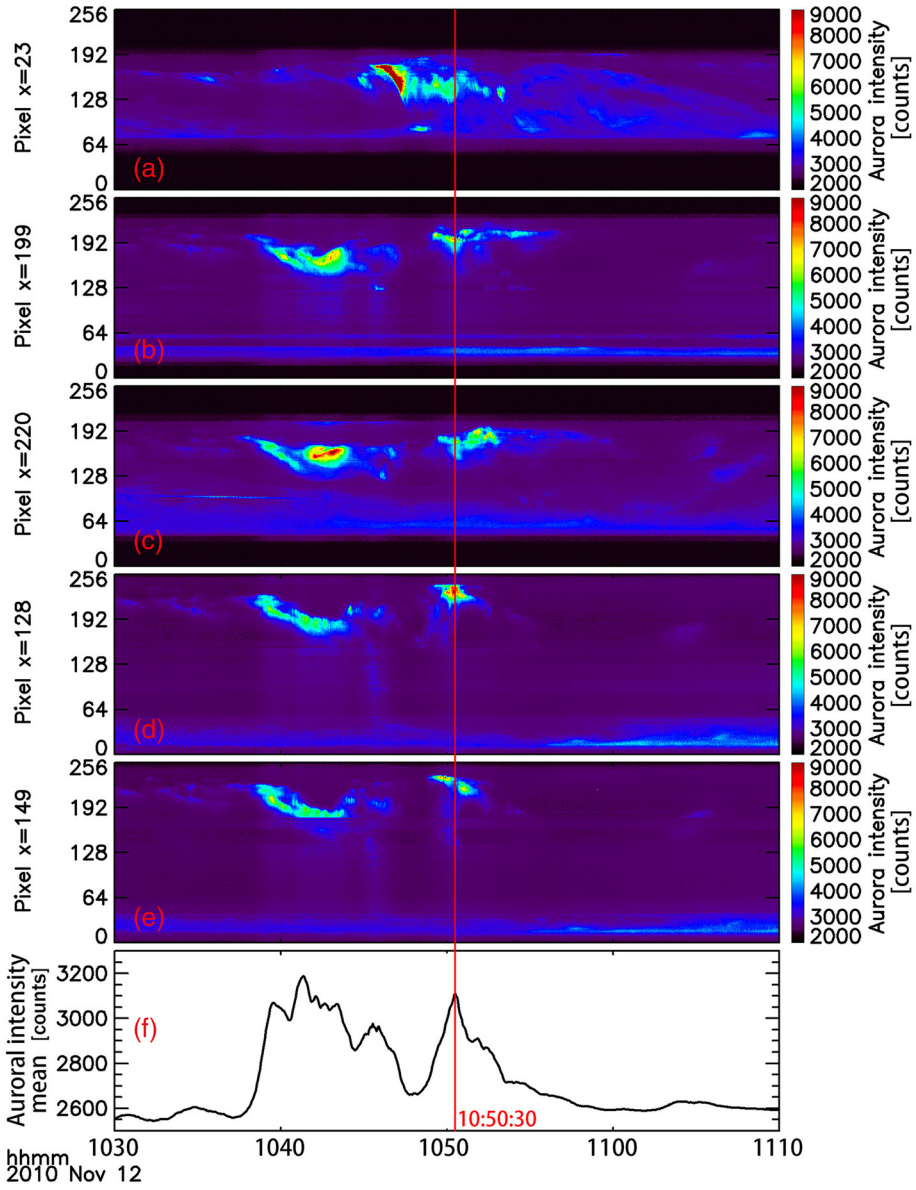

Figure 13. ((a)–(e)): Time variation of auroral intensity along slices ((a)–(e)) taken from Figure 12. The variations of auroral intensity at five slices (as marked in Figure 12) along the time are shown in ((a)–(e)). The bottom panel (f) shows the time variation of the average value of auroral intensity within the red rectangle (as marked in Figure 12). The red vertical line indicates the beginning time of decreased auroral intensity.

consistent with the model in Figure 1. However, sometimes they coexist simultaneously on the dawn side or dusk side. We will enumerate these cases one by one in a future statistical study, in which we will explore the causes of their formation and investigate possible correlations between these two simultaneous vortices. The observation of multiple vortices in response to some SW P_{dyn} events (and not others) suggests that their generation is sensitive to details of the solar wind/magnetosphere interaction during the passage of the pulse, which may be determined by its structure, or prior conditions along the magnetopause. This will form the subject of future modeling studies of these types of events.

3. Summary and Discussion

We have presented two events, in this paper, to study ionospheric reactions shortly after the arrival of a positive SW P_{dyn} pulse. These two events were selected from the OMNI database and were found to exhibit clear EICs vortices and auroral activity in the ionosphere, from THEMIS ground magnetometer and THEMIS ASI optical observations at the GILL and INUV stations. Analysis of the two events showed that the evolution of EICs vortices and the variation of aurora intensity are associated with a chain reaction caused by the SW P_{dyn} sudden increase via FACs generated at flanks of the magnetosphere near the equatorial plane (Shi et al., 2014, 2020). Results from the two events are summarized as below:

1. Within 10 min of SW P_{dyn} pulse arrival at the Earth's magnetosphere, a clockwise EICs vortex is generated on the dawn side and a counterclockwise EICs vortex is generated on the dusk side in the ionosphere
2. Within 10 min of the EICs vortex generation, both upward and downward currents on the dusk/dawn side enhanced/reduced. Therefore, the FACs on the dusk side is mainly upward, and on the dawn side is mainly downward
3. Auroral intensity in the EICs vortex region increased at dusk and decreased at dawn, which is consistent with the mechanism proposed by Shi et al. (2014)

The auroral emission variation corresponds to the duration of the vortex in these two events. For the first case, from the vortex appears at 00:26 UT to disappears at 00:50 UT, the auroral intensity increases from 00:34 UT and decreases form 00:50 UT until the auroral intensity reaches its minimum at 00:59 UT. For the second case, from the vortex appears at 10:48 UT to disappears at 11:02 UT, the auroral intensity decreases form 10:50 UT until the auroral disappear completely at 10:59 UT.

We have focused on the ionospheric responses to a SW P_{dyn} sudden increase in this research. Next, we will study the responses both in the ionosphere and magnetosphere to a negative SW P_{dyn} pulse, and conduct a statistical study of ionospheric vortex events and their auroral response to positive and negative SW P_{dyn} pulses, respectively, to verify whether these responses are common.

Observations and simulations have shown that vortices occur simultaneously in the magnetosphere and ionosphere following the arrival of a SW P_{dyn} pulse. The generation of magnetospheric plasma vortices following a SW P_{dyn} variation was first proposed by Sibeck (1990). Wang et al. (2010) and Samsonov & Sibeck (2013) successively obtained plasma vortices in magnetosphere by global MHD simulations. Later, Shi et al. (2014) and Tian et al. (2016) inferred the simultaneous existence of vortices both in magnetosphere and ionosphere by combining simulation and observation results. Finally, Shi et al. (2020) considered the global response of the ionosphere coupled magnetosphere system and concluded that there was a complete chain reaction between the solar wind dynamic pressure pulse, magnetospheric vortex, FAC, ionospheric vortex, and aurora (as shown in Figure 1). Our results show that the proposed mechanism by Shi et al. (2014) on the whole provides a plausible mechanism for the reduction in auroral intensities at dawn and the increased in auroral intensities at dusk following an increase in SW P_{dyn}. According to the global response model in Figure 1, dusk side auroral intensity increases (as shown in Section 2.1) and dawn side auroral intensity decreases (as shown in Section 2.2), we therefore expect that there is a counterclockwise and clockwise tailward plasma vortex in the magnetosphere, respectively, to provide the upward and downward FAC for the current vortex to produce auroral activity in the ionosphere. Our results also indicate that multiple vortices may be generated following a SW P_{dyn} pulse in some cases, suggesting that details of the solar wind/magnetosphere interaction during the passage of the pulse (over and above that considered by Shi et al., 2020) may also be important. In addition, considering the influences of compressional wave on the formation of magnetospheric plasma vortices, the detailed time sequence of the generation of these phenomena should also be estimated theoretically and observed further. Therefore, in the future work, we plan to start from the magnetospheric responses (compressional wave, vortex, and FAC) caused by the SW P_{dyn} pulse, and afterward to completely demonstrate the coupling process between them and the ionospheric responses (vortex and aurora), and finally give a detailed time sequence of all these phenomena.

Data Availability Statement

The authors acknowledge V. Angelopoulos for use of data from the THEMIS Mission, as well as the use of NASA/GSFC's Space Physics Data Facility's OMNIWeb (or CDAWeb or ftp) service, and OMNI data (https://omniweb.sci.gsfc.nasa.gov/html/ow_data.html or https://omniweb.sci.gsfc.nasa.gov/html/HRO-docum.html). All THEMIS aurorae data can be obtained from http://themis.ssl.berkeley.edu/index.shtml. The equivalent ionospheric currents (EICs) and the spherical elementary current system (SECs) used data from http://vmo.igpp.ucla.edu/data1/SECS/. Dr. Weygand and the SECs archive were supported by NASA THEMIS contract NAS5-02099 and NASA HiDEE award number NNX14AJ77G. I. J. Rae is supported by the Science and Technology Facilities Council (ST/V006320/1), and the Natural Environment Research Council (Grants NE/P017150/1, NE/P017185/2, NE/V002554/2, and NE/V002724/1). The authors thank Zhao Huayu some fruitful help for our work.

Acknowledgments
This work was supported by the National Natural Science Foundation of China (Grants 41731068, 41774172, 41974189, 41941001, and 41961130382) and the Royal Society Newton Advanced Fellowship NAF\R1\191047, the Specialized Research Fund for State Key Laboratories, the young scholar plan of Shandong University at Weihai (2017WHWLJH08).

References

Akasofu, S. I. (1964). The development of geomagnetic storms after a negative sudden impulse. *Planetary and Space Science*, *12*(6), 573–578. http://doi.org/10.1016/0032-0633(64)90004-2

Allan, W., & Poulter, E. M. (1992). ULF waves - their relationship to the structure of the earth's magnetosphere. *Reports on Progress in Physics*, *55*(5), 533–598.

Amm, O. (1997). Ionospheric elementary current systems in spherical coordinates and their application. *Journal of Geomagnetism and Geoelectricity*, *49*(7), 947–955. http://doi.org/10.5636/jgg.49.947

Amm, O. (1998). Method of characteristics in spherical geometry applied to a Harang-discontinuity situation. *Annales Geophysicae*, *16*(4), 413–424. http://doi.org/10.1007/s00585-998-0413-2

Amm, O., & Kauristie, K. (2002). Ionospheric signatures of bursty bulk flows. *Surveys in Geophysics*, *23*(1), 1–32. http://doi.org/10.1023/A:1014871323023

Amm, O., & Viljanen, A. (1999). Ionospheric disturbance magnetic field continuation from the ground to the ionosphere using spherical elementary currents systems. *Earth Planets and Space*, *51*(6), 431–440. http://doi.org/10.1186/BF03352247

Araki, T., & Nagano, H. (1988). Geomagnetic response to sudden expansions of the magnetosphere. *Journal of Geophysical Research*, *93*(A5), 3983. http://doi.org/10.1029/JA093iA05p03983

Birn, J. M., Reader, J., Wang, Y. L., Wolf, R. A., & Hesse, M. (2004). On the propagation of bubbles in the geomagnetic tail. *Annales Geophysicae*, *22*(5), 1773–1786. http://doi.org/10.5194/angeo-22-1773-2004

Carter, B. A., Pradipta, R., Zhang, K., Yizengaw, E., Halford, A. J., & Norman, R. (2015). Interplanetary shocks and the resulting geomagnetically induced currents at the equator. *Geophysical Research Letters*, *42*, 6554–6559. https://doi.org/10.1002/2015gl065060

Degeling, A. W., Rae, I. J., Watt, C. E. J., Shi, Q. Q., Rankin, R., & Zong, Q.-G. (2018). Control of ULF wave accessibility to the inner magnetosphere by the convection of plasma density. *Journal of Geophysical Research: Space Physics*, *123*, 1086–1099. https://doi.org/10.1002/2017JA024874

Degeling, A. W., Rankin, R., & Zong, Q.-G. (2014). Modeling radiation belt electron acceleration by ULF fast mode waves, launched by solar wind dynamic pressure fluctuations. *Journal of Geophysical Research: Space Physics*, *119*, 8916–8928. https://doi.org/10.1002/2013JA019672

Fiori, R. A. D., Boteler, D. H., & Gillies, D. M. (2014). Assessment of GIC risk due to geomagnetic sudden commencements and identification of the current systems responsible. *Space Weather*, *12*, 76–91. https://doi.org/10.1002/2013SW000967

Fukushima, N. (1976). Generalized theorem for no ground magnetic effect of vertical currents connected with Pedersen currents in the uniform-conductivity ionosphere. *Report of Ionosphere and Space Research in Japan*, *30*(1–2), 35–40.

Glassmeier, K.-H., & Heppner, C. (1992). Traveling magnetospheric convection twin-vortices: Another case study, global characteristics, and a model. *Journal of Geophysical Research*, *97*(A4), 3977–3992. http://doi.org/10.1029/91JA02464

Glassmeier, K.-H., Hönisch, M., & Untiedt, J. (1989). Ground-based and satellite-observations of traveling magnetospheric convection twin vortices. *Journal of Geophysical Research*, *94*(A3), 2520–2528. http://doi.org/10.1029/JA094iA03p02520

Hubert, B., Gérard, J. C., Fuselier, S. A., & Mende, S. B. (2003). Observation of dayside subauroral proton flashes with the IMAGE-FUV imagers. *Geophysical Research Letters*, *30*(3), 1145. http://doi.org/10.1029/2002GL016464

Keiling, A., Angelopoulos, V., Runov, A., Weygand, J., Apatenkov, S. V., Mende, S., et al. (2009). Substorm current wedge driven by plasma flow vortices: THEMIS observations. *Journal of Geophysical Research*, *114*, A00C22. http://doi.org/10.1029/2009JA014114

Li, L. Y., Cao, J. B., Zhou, G. C., Yang, J. Y., Yan, C. X., Zhang, T. L., et al. (2008). Shrinkage of magnetosphere observed by TC-1 satellite during the high-speed solar wind stream. *Science in China – Series E: Technological Sciences*, *51*(10), 1695–1703. http://doi.org/10.1007/s11431-008-0258-7

Li, L. Y., Cao, J. B., Zhou, G. C., Zhang, T. L., Zhang, D., Dandouras, I., et al. (2011). Multiple responses of magnetotail to the enhancement and fluctuation of solar wind dynamic pressure and the southward turning of interplanetary magnetic field. *Journal of Geophysical Research*, *116*, A12223. http://doi.org/10.1029/2011JA016816

Li, L. Y., Liu, B., Yu, J., & Cao, J. B. (2017). The rapid responses of magnetosonic waves to the compression and expansion of Earth's magnetosphere. *Geophysical Research Letters*, *44*(22), 11239–11247. http://doi.org/10.1002/2017GL075649

Liou, K., Newell, P. T., Shue, J.-H., Meng, C.-I., Miyashita, Y., Kojima, H., & Matsumoto, H. (2007). "Compression aurora": Particle precipitation driven by long-duration high solar wind ram pressure. *Journal of Geophysical Research*, *112*, A11216. http://doi.org/10.1029/2007JA012443

Liou, K., Newell, P. T., Sotirelis, T., & Meng, C.-I. (2006). Global auroral response to negative pressure impulses. *Geophysical Research Letters*, *33*(11), L11103. http://doi.org/10.1029/2006GL025933

Lui, A. T. Y., Spanswick, E., Donovan, E. F., Liang, J., Liu, W. W., LeContel, O., & Zong, Q.-G. (2010). A transient narrow poleward extrusion from the diffuse aurora and the concurrent magnetotail activity. *Journal of Geophysical Research*, *115*, A10210. http://doi.org/10.1029/2010JA015449

Lyons, L. R., & Fennell, J. F. (1986). Characteristics of auroral electron precipitation on the morningside. *Journal of Geophysical Research*, *91*(A10), 1225–1234. http://doi.org/10.1029/JA091iA10p11225

Mann, I. R., Milling, D. K., Rae, I. J., Ozeke, L. G., Kale, A., Kale, Z. C., & Singer, H. J. (2008). The upgraded CARISMA magnetometer array in THEMIS era. *Space Science Reviews*, *141*(1–4), 413–451. https://doi.org/10.1007/s11214-008-9457-6

Marcia, N., & Raymond, G. (1997). Particle and field signatures of coronal mass ejections in the solar wind. In N. Crooker, J. A. Joselyn, & J. Feynman (Eds.), *Coronal mass ejections*. (pp. 245–251). Washington, DC: AGU.

Marshall, R. A., Dalzell, M., Waters, C. L., Goldthorpe, P., & Smith, E. A. (2012). Geomagnetically induced currents in the New Zealand power network. *Space Weather*, *10*, S08003. https://doi.org/10.1029/2012SW000806

Meurant, M., Gérard, J.-C., Blockx, C., Hubert, B., & Coumans, V. (2004). Propagation of electron and propagation of electron and proton shock-induced aurora and the role of the interplanetary magnetic field and solar wind. *Journal of Geophysical Research*, *109*, A10210. http://doi.org/10.1029/2004JA010453

Meurant, M., Gérard, J.-C., Hubert, B., Blockx, C., Østgaard, N., & Mende, S. B. (2003). Dynamic of global scale electron and proton precipitation induced by a solar wind pressure pulse. *Geophysical Research Letters*, *30*(20), 2032. http://doi.org/10.1029/2003GL018017

Newitt, L., & Coles, R. (2007). *Observatories in Canada. Encyclopedia of Geomagnetism and Paleomagnetism*, 708–748. https://doi.org/10.1007/978-1-4020-4423-6_234

Olmsted, C., & Akasofu, S. I. (1986). A method for determining co-rotating interaction regions in the equatorial plane of the heliosphere from solar wind velocity data. *Journal of Geophysical Research*, *91*(A12), 3689–3693. http://doi.org/10.1029/JA091iA12p13689

Rostoker, G., Kamide, Y., & Winningham, J. D. (1985). Energetic particle precipitation into the high-latitude ionosphere and the auroral electrojets, 3, Characteristics of electron precipitation into the morning sector auroral oval. *Journal of Geophysical Research*, *90*(NA8), 7495–7504. http://doi.org/10.1029/JA090iA08p07495

Russell, C. T., Le, G., Chi, P., Zhou, X.-W., Shue, J.-H., Petrinec, S. M., et al. (2000). The extreme compression of the magnetosphere on May 4, 1998, as observed by the Polar spacecraft. *Advances in Space Research*, *25*(7/8), 1369–1375. http://doi.org/10.1016/S0273-1177(99)00646-8

Russell, C. T., Chi, P. J., Dearborn, D. J., Ge, Y. S., Kuo-Tiong, B., Means, J. D., & Snare, R. C. (2008). THEMIS ground-based magnetometers. *Space Science Reviews*, *141*(1–4), 389–412. https://doi.org/10.1007/s11214-008-9337-0

Russell, C. T., Zhou, X. W., Chi, P. J., Kawano, H., Moore, T. E., Peterson, W. K., et al. (1999). Sudden compression of the outer magnetosphere associated with an ionospheric mass ejection. *Geophysical Research Letters*, *26*(15), 2343–2346. http://doi.org/10.1029/1999GL900455

Samsonov, A. A., & Sibeck, D. G. (2013). Large-scale flow vortices following a magnetospheric sudden impulse. *Journal of Geophysical Research: Space Physics*, *118*(6), 3055–3064. http://doi.org/10.1002/jgra.50329

Samsonov, A. A., Sibeck, D. G., & Imber, J. (2007). MHD simulation for the interaction of an interplanetary shock with the Earth's magnetosphere. *Journal of Geophysical Research*, *112*, A12220. http://doi.org/10.1029/2007JA012627

Samsonov, A. A., Sibeck, D. G., & Yu, Y.-Q. (2010). Transient changes in magnetospheric-ionospheric currents caused by the passage of an interplanetary shock: Northward interplanetary magnetic field case. *Journal of Geophysical Research*, *115*, A05207. http://doi.org/10.1029/2009JA014751

Sato, N., Murata, Y., Yamagishi, H., Yukimatu, A. S., Kikuchi, M., Watanabe, M., et al. (2001). Enhancement of optical aurora triggered by the solar wind negative impulse (SI^{-}). *Geophysical Research Letters*, *28*(1), 127–130. http://doi.org/10.1029/2000GL003742

Sun, T. R., Wang, C., Zhang, J. J., Pilipenko, V. A., Wang, Y., & Wang, J. Y. (2015). The chain response of the magnetospheric and ground magnetic field to interplanetary shocks. *Journal of Geophysical Research: Space Physics*, *120*(1), 157–165. http://doi.org/10.1002/2014JA020754

Shi, Q. Q., Hartinger, M. D., Angelopoulos, V., Tian, A. M., Fu, S. Y., Zong, Q.-G., et al. (2014). Solar wind pressure pulse-driven magnetospheric vortices and their global consequences. *Journal of Geophysical Research: Space Physics*, *119*(6), 4274–4280. http://doi.org/10.1002/2013JA019551

Shi, Q. Q., Hartinger, M. D., Angelopoulos, V., Zong, Q.-G., Zhou, X.-Z., Zhou, X.-Y., et al. (2013). THEMIS observations of ULF wave excitation in the nightside plasma sheet during sudden impulse events. *Journal of Geophysical Research: Space Physics*, *118*, 284–298. https://doi.org/10.1029/2012JA017984

Shi, Q. Q., Shen, X.-C., Tian, A. M., Degeling, A. W., Zong, Q.-G., Fu, S. Y., et al., & ISBN. (2020). Magnetosphere response to solar wind dynamic pressure change: Vortices, ULF waves and aurorae. Dayside magnetosphere interactions. Q.-G. Zong, P. Escoubet, D. Sibeck, G. Le, & H. Zhang (Eds.), *Geophysical monograph*. 248. (pp. 79–97). American Geophysical Union (ISBN: 978-1-119-50963-9). https://doi.org/10.1002/9781119509592.ch5

Shi, Q. Q., Zong, Q.-G., Fu, S. Y., Dunlop, M. W., Pu, Z. Y., Parks, G. K., et al. (2013). Solar wind entry into the high-latitude terrestrial magnetosphere during geomagnetically quiet times. *Nature Communications*, *4*, 1466. https://doi.org/10.1038/ncomms2476

Shi, Q. Q., Zong, Q.-G., Zhang, H., Pu, Z. Y., Fu, S. Y., Xie, L., et al. (2009). Cluster observations of the entry layer equatorward of the cusp under northward interplanetary magnetic field. *Journal of Geophysical Research*, *114*, A12219. https://doi.org/10.1029/2009JA014475

Sibeck, D. G. (1990). A model for the transient magnetospheric response to sudden solar wind dynamic pressure variations. *Journal of Geophysical Research*, *95*(A4), 3755–3771. http://doi.org/10.1029/JA095iA04p03755

Smith, A. W., Freeman, M. P., Rae, I. J., & Forsyth, C. (2019). The influence of sudden commencements on the rate of change of the surface horizontal magnetic field in the United Kingdom. *Space Weather*, *17*, 1605–1617. https://doi.org/10.1029/2019SW002281

Takeuchi, T., Araki, A., Viljanen, A., & Watermann, J. (2002). Geomagnetic negative sudden impulses: Interplanetary causes and polarization distribution. *Journal of Geophysical Research*, *107*(A7), 1096. http://doi.org/10.1029/2001JA900152

Tian, A. M., Shen, X. C., Shi, Q. Q., Tang, B. B., Nowada, M., Zong, Q. G., & Fu, S. Y. (2016). Dayside magnetospheric and ionospheric responses to solar wind pressure increase: Multispacecraft and ground observations. *Journal of Geophysical Research: Space Physics*, *121*(11), 10813–10830. http://doi.org/10.1002/2016JA022459

Vorobjev, V. G. (1974). SC-related auroral effects. *Geomagnetism and Aeronomy*, *14*(1), 90–92.

Wang, C., Sun, T. R., Guo, X. C., & Richardson, J. D. (2010). Case study of nightside magnetospheric magnetic field response to interplanetary shocks. *Journal of Geophysical Research*, *115*, A10247. http://doi.org/10.1029/2010JA015451

Weygand, J., & Wing, S. (2016). Comparison of DMSP and SECS region-1 and region-2 ionospheric current boundary. *Journal of Atmospheric and Solar-Terrestrial Physics*, *143*, 8–13. http://doi.org/10.1016/j.jastp.2016.03.002

Weygand, J. M. (2009a). *Equivalent ionospheric currents (EICs) derived using the spherical elementary currents systems (SECS) technique at 10 sec resolution in geographic coordinates [data set]*. UCLA. http://doi.org/10.21978/P8D62B

Weygand, J. M. (2009b). *Spherical elementary current (SEC) amplitudes derived using the spherical elementary currents systems (SECS) technique at 10 sec resolution in geographic coordinates [data set]*. UCLA. http://doi.org/10.21978/P8PP8X

Weygand, J. M., Amm, O., Viljanen, A., Angelopoulos, V., Murr, D., Engebretson, M. J., et al. (2011). Application and validation of the spherical elementary currents systems technique for deriving ionospheric equivalent currents with the North American and Greenland ground magnetometer arrays. *Journal of Geophysical Research*, *116*, A03305. http://doi.org/10.1029/2010JA016177

Wilken, B., Goertz, C. K., Baker, D. N., Higbie, P. R., & Fritz, T. A. (1982). The SSC on July 29, 1997, and its propagation within the magnetosphere. *Journal of Geophysical Research*, *87*(NA8), 5901–5910. http://doi.org/10.1029/JA087iA08p05901

Winterhalter, D., Smith, E. J., Burton, M. E., Murphy, N., & McComas, D. J. (1994). The heliospheric plasma sheet. *Journal of Geophysical Research*, *99*(A4), 6667–6680. http://doi.org/10.1029/93JA03481

Yang, B., Zong, Q.-G., Wang, Y. F., Fu, S. Y., Song, P., Fu, H. S., & Reme, H. (2010). Cluster observations of simultaneous resonant interactions of ULF waves with energetic electrons and thermal ion species in the inner magnetosphere. *Journal of Geophysical Research*, *115*, A02214. https://doi.org/10.1029/2009JA014542

Yao, Z. H., Pu, Z. Y., Fu, S. Y., Angelopoulos, V., Kubyshkina, M., Xing, X., et al. (2012). Mechanism of substorm current wedge formation: THEMIS observations. *Geophysical Research Letters*, *39*, L13102. http://doi.org/10.1029/2012GL052055

Zhao, H., Zhou, X.-Z., Zong, Q.-G., Weygand, J. M., Shi, Q., Liu, Y., et al. (2019). Small-scale aurora associated with magnetospheric flow vortices after a solar wind dynamic pressure decrease. *Journal of Geophysical Research: Space Physics*, *124*(5), 3303–3311. http://doi.org/10.1029/2018JA026234

Zhao, H. Y., Shen, X. C., Tang, B. B., Tian, A. M., Shi, Q. Q., Weygand, J. M., et al. (2016). Magnetospheric vortices and their global effect after a solar wind dynamic pressure decrease. *Journal of Geophysical Research: Space Physics*, *121*(2), 1071–1077. http://doi.org/10.1002/2015JA021646

Zhang, X. Y., Zong, Q.-G., Wang, Y. F., Zhang, H., Xie, L., Fu, S. Y., et al. (2010). ULF waves excited by negative/positive solar wind dynamic pressure impulses at geosynchronous orbit. *Journal of Computational Physics*, *115*, A10221. https://doi.org/10.1029/2009JA015016

Zhou, X. Z., Ge, Y. S., Angelopoulos, V., Runov, A., Liang, J., Xing, X., et al. (2012). Dipolarization fronts and associated auroral activities: 2. Acceleration of ions and their subsequent behavior. *Journal of Geophysical Research*, *117*, A10227. https://doi.org/10.1029/2012JA017677

Zhou, X.-Y., Strangeway, R. J., Anderson, P. C., Sibeck, D. G., Tsurutani, B. T., Haerendel, G., et al. (2003). Shock aurora: FAST and DMSP observations. *Journal of Geophysical Research*, *108*(A4), 8019. http://doi.org/10.1029/2002JA009701

Zhou, X. Y., & Tsurutani, B. T. (1999). Rapid intensification and propagation of the dayside aurora: Large-scale interplanetary pressure pulses (fast shocks). *Geophysical Research Letters*, *26*(8), 1097–1100. http://doi.org/10.1029/1999GL900173

Zhou, X. Y., & Tsurutani, B. T. (2001). Interplanetary shock triggering of nightside geomagnetic activity: substorms, pseudo breakups, and quiescent events. *Journal of Geophysical Research*, *106*(A9), 18957–18967. http://doi.org/10.1029/2000JA003028

Zong, Q.-G., Fritz, T. A., Zhang, H., Korth, A., Daly, P. W., Dunlop, M. W., et al. (2004). Triple cusps observed by Cluster: Temporal or spatial effect? *Geophysical Research Letters*, *31*, L09810. https://doi.org/10.1029/2003GL019128

Zong, Q.-G., Reinisch, B. W., Song, P., Wei, Y., & Galkin, I. A. (2010). Dayside ionospheric response to the intense interplanetary shocks-solar wind discontinuities: Observations from the digisonde global ionospheric radio observatory. *Journal of Geophysical Research*, *115*, A06304. http://doi.org/10.1029/2009JA014796

Zong, Q.-G., Wang, Y. F., Yang, B. A., Fu, S. Y., Pu, Z. Y., Xie, L., & Fritz, T. A. (2008). Recent progress on ULF wave and its interactions with energetic particles in the inner magnetosphere. *Science in China – Series E: Technological Sciences*, *51*(10), 1620–1625. https://doi.org/10.1007/s11431-008-0253-z

Zong, Q.-G., Wang, Y. F., Zhang, H., Fu, S. Y., Zhang, H., Wang, C. R., et al. (2012). Fast acceleration of inner magnetospheric hydrogen and oxygen ions by shock induced ULF waves. *Journal of Geophysical Research*, *117*, A11206. https://doi.org/10.1029/2012JA018024

Zong, Q.-G., Zhou, X.-Z., Wang, Y. F., Li, X., Song, P., Baker, D. N., et al. (2009). Energetic electron response to ULF waves induced by interplanetary shocks in the outer radiation belt. *Journal of Geophysical Research*, *114*, A10204. http://doi.org/10.1029/2009JA014393